Optics Letters

Visibly transparent multifunctional camouflage coating with efficient thermal management

Sandeep Kumar Chamoli[1,2,4] and Wei Li[1,3,*]

[1]GPL Photonics Laboratory, State Key Laboratory of Luminescence and Applications, Changchun Institute of Optics, Fine Mechanics and Physics, Chinese Academy of Sciences, Changchun 130033, China
[2]School of Chemical and Biotechnology Engineering, Nanyang Technological University, 637457, Singapore
[3]University of Chinese Academy of Sciences, Beijing 100049, China
[4]sandeep.chamoli@ntu.edu.sg
*weili1@ciomp.ac.cn

Received 3 May 2023; revised 8 June 2023; accepted 15 June 2023; posted 17 July 2023; published 10 August 2023

Camouflage technology has attracted growing interest in many thermal applications. In particular, high-temperature infrared (IR) camouflage is crucial to the effective concealment of high-temperature objects but remains a challenging issue, as the thermal radiation of an object is proportional to the fourth power of temperature. Here, we proposed a coating to demonstrate high-temperature IR camouflage with efficient thermal management. This coating is a combination of hyperbolic metamaterial (HMM), gradient epsilon near zero (G-ENZ) material, and polymer. HMM makes the coating transparent in the visible range (300–700 nm) and highly reflective in the IR region, so it can serve as a thermal camouflage in the IR. G-ENZ and polymer support BE mode (at higher angles ~50° to 90° in the 11–14 μm atmospheric window) and vibrational absorption band (in 5–8 μm non-atmospheric for all angles), respectively. So it is possible to achieve efficient thermal management through radiative cooling. We calculate the temperature of the object's surface, considering the emissivity characteristics of the coating for different heating temperatures. A combination of silica aerogel and coating can significantly reduce the surface temperature from 2000 K to 750 K. The proposed coating can also be used in the visible transparent radiative cooling due to high transmission in the visible, high reflection in the near-IR (NIR), and highly directional emissivity in the atmospheric window at higher angles, and can therefore potentially be used as a smart window in buildings and vehicles. Finally, we discuss one more potential future application of such a multifunctional coating in water condensation and purification.

https://doi.org/10.1364/OL.494539

Camouflage is a concealment technique that uses multiple materials, colors, or illuminations [1]. A method for doing this would be to make objects or targets difficult to detect or make them look like something else. Camouflage technology can be divided into two groups based on the physical mechanisms behind it: color-based camouflage and thermal-based camouflage. A color camouflage technique matches an object's appearance to that of the background by tuning the reflection or transmission of light in the visible or near-infrared range (NIR) part of the electromagnetic (EM) spectrum [2]. However, thermal camouflage controls the thermal emission radiation to maintain a balance between an object's temperature and the background and belongs to the IR region of the EM spectrum. IR camouflage can hide an object's signature in the IR spectrum and make it inactive to possible potential risks that can detect it with IR detector equipment, such as thermal imaging systems, heat-seeking missiles, and satellites that can detect IR missiles [3]. It should have low emittance between 3 to 5 μm in the middle IR window (MWIR), and 8 to 14 μm in the long wave IR window (LWIR) against thermal imagers and heat-seeking missiles [4].

Plank's law states that an object whose temperature exceeds absolute zero emits thermal radiation, which in most cases falls within the region of mid-IR [5]. Surface emittance (ε) and temperature (T)determine the amount of thermal radiation (Q) of an object and given by $Q = \sigma T^4$. This implies that an object's surface emittance can be manipulated, or its surface temperature may be manipulated, to achieve IR camouflage. Consequently, thermal camouflage can be fooled by thermal imagers, which compare the differences in temperature between the object and the background to distinguish them. A number of nanophotonic designs have been proposed based on nanostructure [6–8] or metal-semiconductor multilayer [9–13] film for controlling thermal radiation with low surface emittance across the entire IR spectrum. In addition, wavelength-selective emitters have been applied to mitigate heat instability without affecting IR camouflage in the non-atmospheric window (5–8 μm) via radiative cooling [12,14]. There are a number of challenges involved in manipulating EM waves for thermal camouflage with efficient heat management, since one has to consider a vast spectrum ranging from visible to IR, and also different principles of camouflage.

In this Letter, we propose a concept of visibly transparent camouflage coating (VT-CC) with efficient thermal management. Figure 1 illustrates the concept of VT-CC, which is transparent in the visible range (300–700 nm), highly reflective in the MWIR range (3–5 μm), and highly reflective in the LWIR range (8–14 μm) if the viewing angle is lower, say from normal to 45 degrees. Meanwhile, heat instability is maintained with high

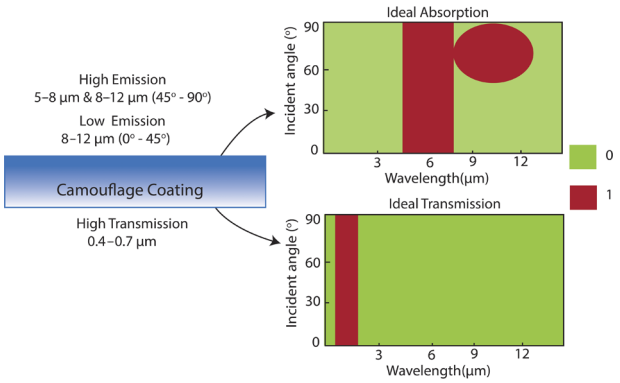

Fig. 1. Concept of visibly transparent camouflage coating with efficient thermal management, VT-CC: Illustration of a thermal camouflage coating on top of an object or target that needs to be hidden. Because the atmosphere is opaque at 5–8 μm, this window can be used for radiative cooling. The atmosphere in the 8–14 μm window is transparent, so we want low absorption or emission in this window for lower angles, such as 0° to 45°. However, high emissions at higher angles, such as 45° to 90°, can be useful in thermal management through radiative cooling. Hence, we aim to create a thermal camouflage coating that can transmit between 300 nm and 700 nm, absorb 5–8 μm for all angles, absorb 8–14 μm from 45° to 0°, and have a high reflection in the remainder of the EM range, for example from 0.7 to 5 μm and from 8 to 14 μm at 0° to 45°.

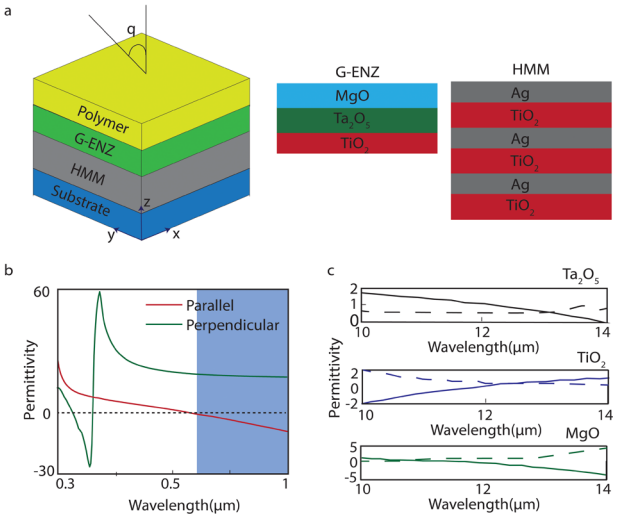

Fig. 2. A proposed design for VT-CC. (a) Schematic of a multilayer coating, consisting of HMM, G-ENZ, and polymer at the top. The HMM consist of three bilayers of Ag–TiO_2, the G-ENZ consists of MgO–Ta_2O_5–TiO_2. (b) dispersion of Ag–TiO_2 HMM. (c) Real (solid) and imaginary (dashed) parts of permittivities of three polaritonic oxide materials Ta_2O_5, TiO_2, and MgO, showing slowly varying permittivity that crosses zero at complementary wavelengths in the LWIR part of the EM spectrum.

emission/absorption in 5–8 μm and 8–14 μm but at higher angles from 50° to 90°.

We design a multilayer coating that can fulfill all the requirements of VT-CC, as shown in Fig. 2(a). The design considerations are as follows: (1) to make the coating visibly transparent and reflective in the whole LWIR and MWIR we used a hyperbolic metamaterial (HMM) [15] made of silver (Ag) and titanium dioxide (TiO_2); (2) to make the coating emissive in the atmospheric transmission window in the range 8–14 μm at higher angles (45°–90°) we used the concept of gradient epsilon near zero (G-ENZ) [16] materials [TiO_2–Ta_2O_5 (titanium pentaoxide)–MgO (magnesium oxide)] which support the Berreman (BE) mode [17]; and (3) to make the coating emissive in the the 5–8 μm window we used polyetherimid (PEI) polymer, which features vibrational properties within the 5–8 μm window, making the coating absorbing in this region [18]. The proposed VT-CC is significantly less cost-effective than previously proposed camouflage designs based on nano-structures or thin films. Figure 2(b) show parallel ($\varepsilon_\parallel$) and perpendicular ($\varepsilon_\perp$) permittivity of HMM calculated using the following expressions, where the blue shaded region is showing the hyperbolic region or optical topological transition from elliptical to hyperbolic dispersion in proposed Ag–TiO_2 HMM [15,19]:

$$\varepsilon_\parallel = f_m\varepsilon_m + f_d\varepsilon_d \tag{1}$$

$$\varepsilon_\perp = \frac{\varepsilon_m\varepsilon_d}{f_m\varepsilon_m + f_d\varepsilon_d}, \tag{2}$$

where ε_d and ε_m are the complex permittivities of TiO_2 and Ag, $f_m = \frac{t_m}{t_m+t_d}$ is the fill fraction of Ag, and f_d=1–f_m is the fill fraction of TiO_2, which depend respectively on the thickness of Ag (i.e., t_m) and the thickness of TiO_2 (i.e., t_d). The total thickness of t_m+t_d makes a unit cell. We have used three unit cells. Ag is 10 nm thick and TiO_2 is 20 nm thick, so each unit cell is 30 nm thick, and f_m and f_d are respectively 33% and 66% of the total. So it's evident from Fig. 2(b) that HMM behaves as a metal above 700 nm and as a dielectric below 700 nm, which makes the coating visibly transparent and reflecting in the IR region. In Fig. 2(c), the permittivity function of the three polaritonic ENZ oxide materials (Ta_2O_5 -TiO_2-MgO) is plotted. Layering them produces a G-ENZ because of their complementary resonances in the LWIR part of the spectrum from 11 to 14 μm. The concept of G-ENZ has been introduced recently to overcome the narrowband absorption in ENZ materials by defining the permittivity of materials whose resonance poles change frequency as they move through space [17]:

$$\varepsilon(\omega,d) = \varepsilon_\infty\left(1 + \frac{\omega_L^2-\omega_T^2}{\omega_T^2-\left(\omega-\left(\frac{d}{D}\right)\omega_{range}\right)^2 - i\gamma\left(\omega-\left(\frac{d}{D}\right)\omega_{range}\right)}\right) \quad 0 \le d \le D, \tag{3}$$

where $\omega_{range} = \omega_L - \omega_T$ are the frequencies of out-of-phase atomic lattice vibrations with wave vectors parallel and perpendicular to the incident field, ε_∞ represents the permittivity at infinite frequencies, γ represents the damping rate, and d represents the depth within the gradient ENZ film bounded by zero and the thickness of the film D. As shown in Fig. 2(c), each ENZ material crosses zero at a different frequency in the depth direction. The absorption is related to the Im[ε] and Re[ε] as follows [17] (see note 1 in Supplement 1 for more details):

$$A(r,\omega) = 0.5\omega\,\mathrm{Im}[\varepsilon(\omega)]\left|\frac{E_o(r,\omega)}{\mathrm{Re}[\varepsilon(\omega)]}\right|^2. \tag{4}$$

It is evident from Eq. (4) that absorption is strongly enhanced when Re[ε] approaches zero. When Re[ε] approaches zero, Im[ε] also has a significant effect on the absorption value, and the stronger Im[ε] gets, the wider the angular width and the higher the absorption value [17]. The transfer matrix method

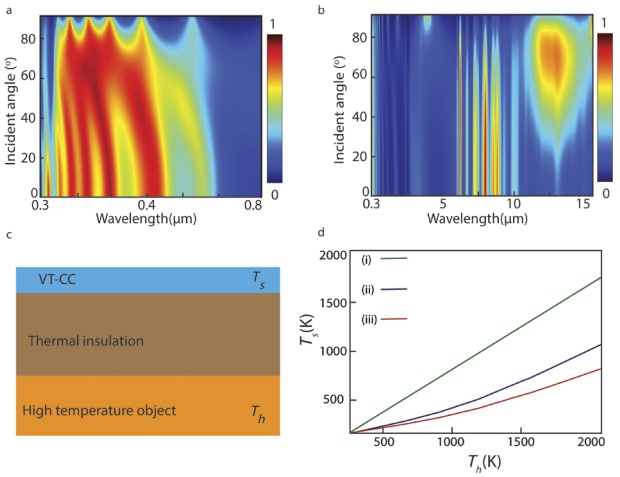

Fig. 3. Simulation & setup to calculate the VT-CC surface temperature. (a) Average transmission from VT-CC as a function of wavelength and incident angle. (b) Average absorption from VT-CC as a function of wavelength and incident angle. (c) Scheme for simulation setup showing practical measurement setup to calculate the temperature of coating. (d) Surface temperatures of VT-CC for different heating temperatures: (i) radiative cooling, using only thermal emission characteristic of VT-CC in 5–8 μm and 8–12 μm in the angular range 50° to 90°; (ii) with only thermal insulation; and (iii) with insulation and radiative cooling together.

(TMM) in finite-difference time-domain (FDTD) is used to simulate average absorption and transmission (for s and p polarizations) using the complex refractive index of each layer of VT-CC [20,21]. Figure 3(a) shows average transmission through VT-CC, as expected the design is highly transmissive in the 400–700 nm range and highly reflecting after 700 nm due to HMM. Figure 3(b) shows the average absorption spectra of VT-CC as a function of wavelength and incident angle, there is clear broad absorption in the 10–14 μm range from 45°–90° due to the BE mode being supported by G-ENZ, being located near the material resonance pole [22,23]. The thicknesses of TiO_2, Ta_2O_5, and MgO are 100 nm, 250 nm, and 180 nm respectively. Also, absorption due to PEI from 5 to 8 μm corresponding to the stretching vibrations of *C* and *N* atoms as well as the vibrations of aromatic rings (see Fig. 1 in Supplement 1) [18]. The thickness of PEI is 500 nm. Therefore, utilizing the absorption band in the wavelengths range 5 to 8 μm and 8 to 12 μm provides opportunities to utilize radiative cooling [24], which leads to improved thermal management in addition to thermal camouflage. Also, PEI is a very useful polymer material, which is used for many other applications due to its thermoplastic, anti-corrosive, high strength, and excellent thermal stability characteristics [25,26]. So we successfully proposed a practical coating to perform the concept of the VT-CC with high thermal management.

Next, we perform the heat transfer and radiative cooling simulation to calculate the temperature rise at the top surface of VT-CC considering real experimental measurement geometry, as shown in Fig. 3(c). A boundary condition at the bottom surface is the temperature of the surface of the object being camouflaged and considered convectively heated with the variable temperature of T_h as follows [12]:

$$-k\left.\frac{dT}{dZ}\right|_{z=0} = h[T_h - T(Z=0)], \tag{5}$$

where k represents thermal conductivity, h represents the heat transfer coefficient, and T_h is the convective heating temperature. The thermal insulator layer is 1-cm-thick silica aerogel with very low k ~0.017 W/mK at 400 K. The upper surface is subjected to natural convection boundary conditions along with radiative heat dissipation in the 5–8 μm and 8–12 μm ranges from 50° to 90°. Also, the convection flow is set to be external on a horizontal plate with an upside down direction. We assume t is the thickness of the thermal insulator, so $z = t$ at position z:

$$-k\left.\frac{dT}{dZ}\right|_{z=t} = h_{conv}[T_h - T(Z=t)] \tag{6}$$

$$h_{conv} = \frac{k}{L}0.54Ra_L^{1/4}, \tag{7}$$

where L represents a characteristic length of the geometry, T_{amb} represents ambient temperature, and Ra_L shows Rayleigh's number at a given value of L. In these boundary conditions, surface temperatures T_s are compared under radiative cooling in the 5–8 μm and 8–12 μm ranges at higher angles 50° to 90°, thermal insulation, and their combined effect. The calculated T_s for three cases (i) through radiative cooling: using only thermal emission characteristic of VT-CC in 5–8 μm and 8–12 μm in the angular range 50° to 90°; (ii) with only thermal insulation; and (iii) with thermal insulation and radiative cooling together. As shown in Fig. 3(d), T_s is most reduced in case (iii), which combines case (i) and case (ii), at the highest heating temperature T_h of 2000 K, where the surface temperature decreases with only radiative cooling, that with only thermal insulation, and their combination is 157 K, 967 K, and 1260 K, respectively. Case (i) becomes more significant as T_h increases above 800 K, because radiation depends on the fourth power of temperature, becoming more dominant at higher T_h and significantly reducing T_s. Hence, thermal insulation and radiation from a non-atmospheric window combined with radiation from an atmospheric window can reduce the object's temperature and improve its IR camouflage with efficient thermal management.

Finally, we would like to discuss the potential future applications of such a coating. First, considering the extensive use of glass windows in modern architecture and smart city environments, the proposed coating could potentially be used in building windows to perform visibly transparent radiative cooling [27]. This coating can also be used on vehicles to reduce unwanted heating. For instance, this coating could be applied to a car parked under direct sunlight to reduce unwanted heating. Secondly, such a coating can be used for condensation and purification of water, as shown schematically in Fig. 4(a). The coating utilized in this study consists of a combination of materials, including SiO_2, Si_3N_4, and SiO [see Fig. 4(b)]. This composition allows the coating to effectively transmit the solar spectrum in the visible range to the IR region, enabling efficient heating of water. Additionally, the presence of to SiO_2, Si_3N_4, and SiO introduces phononic vibrational absorption characteristics, which contribute to the coating's ability to perform radiative cooling (up to ~7° C below ambient under direct sunlight) [28,29]. The radiative cooling property of the transparent coating plays a crucial role in facilitating condensation. When the coated surface is cooler than the ambient air, it creates a favorable temperature gradient that promotes water vapor condensation (see note 2 in Supplement 1 for further details on mechanism). Figures 4(c) and 4(d) show average transmission and absorption,

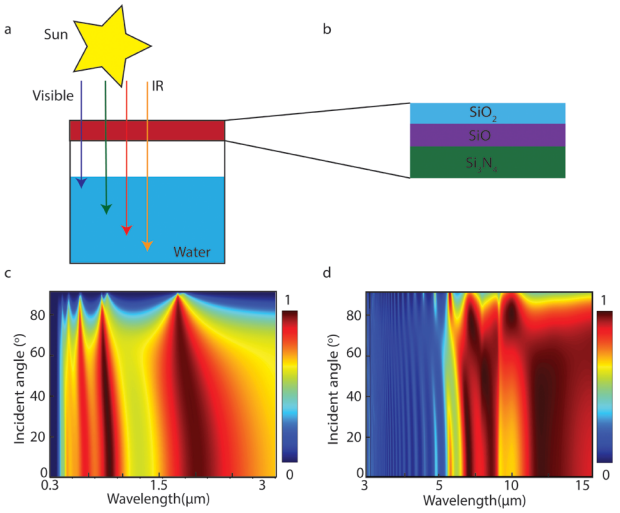

Fig. 4. Water condensation and purification using a visibly and IR transparent coating. (a) Schematic showing the Sun heating water in a water container coated with a coating that allows visible light in and reflects IR. (b) Coating consists of radiative cooling materials such as Si_3N_4, SiO, and SiO_2. (c) Average transmission from the coating as a function of incident angle and wavelength. (d) Average absorption from the coating as a function of incident angle and wavelength.

respectively, for a coating as a function of incident wavelength and angle.

In conclusion, we proposed a cost-effective multilayer coating characterized by multi-functionals, such as visibly transparent, reflecting in IR, and emissive in the 5–8 μm and 10–14 μm ranges at higher angles. First, HMM offers transparency in the visible range and high reflection in the whole IR EM spectrum, i.e., low emittance. Second, G-ENZ layers provide high emissions at higher angles of 50° to 90° in the atmospheric transmission window (10–14 μm) which allows thermal management through radiative cooling. Third, the vibrational absorption band of PEI in non-atmospheric windows (5–8 μm) provides thermal management through radiative cooling. A simulation of the coating surface temperature was performed in three cases: only radiative cooling, only silica aerogel, and a combination of both for different heating temperatures. With radiative cooling, silica aerogel, and their combination, the surface temperature decreases to 157 K, 967 K, and 1260 K, respectively, at the highest heating temperature of $T_h = 2000$ K. The proposed coating is better than the previously proposed nanostructure or thin-film design in terms of cost, fabrication, and functionality [4,9–13,30,31]. Finally, we discussed the potential applications of such a multifunctional coatings in the radiative cooling of smart windows, as well as water condensation and purification.

Funding. National Natural Science Foundation of China (62134009, 62121005); Jilin Provincial Science & Technology Development Project (YDZJ202102CXJD002).

Acknowledgments. This work was supported by the National Natural Science Foundation of China [grant no. 62134009, 62121005] and Jilin Provincial Science & Technology Development Project [grant no. YDZJ202102CXJD002]

Disclosures. The authors declare no conflicts of interest.

Data availability. Data underlying the results presented in this paper are not publicly available at this time but may be obtained from the authors upon reasonable request.

Supplemental document. See Supplement 1 for supporting content.

REFERENCES

1. T. Han, X. Bai, J. T. L. Thong, B. Li, and C. W. Qiu, Adv. Mater. **26**, 1731 (2014).
2. Y. Ying, B. Ma, J. Yu, Y. Huang, P. Ghosh, W. Shen, M. Qiu, and Q. Li, Laser Photonics Rev. **16**, 2200018 (2022).
3. X. Xie, X. Li, M. Pu, X. Ma, K. Liu, Y. Guo, and X. Luo, Adv. Funct. Mater. **28**, 1706673 (2018).
4. H. Zhu, Q. Li, C. Tao, Y. Hong, Z. Xu, W. Shen, S. Kaur, P. Ghosh, and M. Qiu, Nat. Commun. **12**, 1805 (2021).
5. W. Li and S. Fan, Opt. Express **26**, 15995 (2018).
6. Y. Qu, Q. Li, K. Du, L. Cai, J. Lu, and M. Qiu, Laser Photonics Rev. **11**, 1700091 (2017).
7. M. J. Moghimi, G. Lin, and H. Jiang, Adv. Eng. Mater. **20**, 1800038 (2018).
8. T. Liu, C. Guo, W. Li, and S. Fan, eLight **2**, 25 (2022).
9. L. Peng, D. Liu, H. Cheng, S. Zhou, and M. Zu, Adv. Opt. Mater. **6**, 1801006 (2018).
10. Y. Qu, Q. Li, L. Cai, M. Pan, P. Ghosh, K. Du, and M. Qiu, Light: Sci. Appl. **7**, 26 (2018).
11. K. Du, Q. Li, Y. Lyu, J. Ding, Y. Lu, Z. Cheng, and M. Qiu, Light: Sci. Appl. **6**, e16194 (2016).
12. H. Zhu, Q. Li, C. Zheng, Y. Hong, Z. Xu, H. Wang, W. Shen, S. Kaur, P. Ghosh, and M. Qiu, Light: Sci. Appl. **9**, 60 (2020).
13. Z. Xu, Q. Li, K. Du, S. Long, Y. Yang, X. Cao, H. Luo, H. Zhu, P. Ghosh, W. Shen, and M. Qiu, Laser Photonics Rev. **14**, 1900162 (2020).
14. T. Yokoyama, T. D. Dao, K. Chen, S. Ishii, R. P. Sugavaneshwar, M. Kitajima, and T. Nagao, Adv. Opt. Mater. **4**, 1987 (2016).
15. S. K. Chamoli, M. ElKabbash, J. Zhang, and C. Guo, Opt. Lett. **45**, 1671 (2020).
16. A. Nemati, Q. Wang, N. S. S. Ang, W. Wang, M. Hong, and J. Teng, Opto-Electron. Adv. **4**, 200088 (2021).
17. J. Xu, J. Mandal, and A. P. Raman, Science **372**, 393 (2021).
18. X. Zhang, J. Qiu, J. Zhao, X. Li, and L. Liu, J. Quant. Spectrosc. Radiat. Transf. **252**, 107063 (2020).
19. L. Y. Beliaev, O. Takayama, P. N. Melentiev, and A. V. Lavrinenko, Opto-Electron. Adv. **4**, 210031 (2021).
20. S. K. Chamoli, G. Verma, S. C. Singh, and C. Guo, Nanoscale **13**, 1311 (2021).
21. S. K. Chamoli, G. Verma, and S. C. Singh, Nanotechnology **32**, 095207 (2021).
22. W. D. Newman, C. L. Cortes, J. Atkinson, S. Pramanik, R. G. Decorby, and Z. Jacob, ACS Photonics **2**, 2 (2015).
23. J. Rensberg, Y. Zhou, S. Richter, C. Wan, S. Zhang, P. Schöppe, R. Schmidt-Grund, S. Ramanathan, F. Capasso, M. A. Kats, and C. Ronning, Phys. Rev. Appl. **8**, 014009 (2017).
24. M. Lee, G. Kim, Y. Jung, K. R. Pyun, J. Lee, B. Kim, and S. H. Ko, Light: Sci. Appl. **12**, 134 (2023).
25. B. Shen, W. Zhai, M. Tao, J. Ling, and W. Zheng, ACS Appl. Mater. Interfaces **5**, 11383 (2013).
26. B. Polyetherimide, M. Rajagopalan, I. Oh, R. Smalley, and R. Curl, ACS Nano **5**, 2248 (2011).
27. M. Kim, D. Lee, S. Son, Y. Yang, H. Lee, and J. Rho, Adv. Opt. Mater. **9**, 2002226 (2021).
28. S. Chamoli, W. Li, F. Mechanics, and M. Elkabbash, Nanophotonics **11**, 3709 (2022).
29. S. Fan and W. Li, Nat. Photonics **16**, 182 (2022).
30. T. Kim, E. S. Yu, Y. G. Bae, J. Lee, I. S. Kim, S. Chung, S. Y. Lee, and Y. S. Ryu, Light: Sci. Appl. **9**, 175 (2020).
31. L. Xiao, H. Ma, J. Liu, W. Zhao, Y. Jia, Q. Zhao, K. Liu, Y. Wu, Y. Wei, S. Fan, and K. Jiang, Nano Lett. **15**, 8365 (2015).